



Bistable composite laminates: Effects of laminate composition on cured shape and response to thermal load

Peter F. Giddings^{a,*}, Christopher R. Bowen^a, Aki I.T. Salo^b, Hyunsun A. Kim^a, Alan Ive^a

^aDepartment of Mechanical Engineering, University of Bath, Bath, BA2 7AY, United Kingdom

^bSport and Exercise Science, University of Bath, Bath, BA2 7AY, United Kingdom

ARTICLE INFO

Article history:

Available online 1 September 2009

Key words:

Composite structures
Bistable laminates
Finite element
Experimental mechanics
Thermal stress

ABSTRACT

This paper develops a finite element (FE) approach using commercial ANSYS V11.0 software to accurately predict the cured shape of bistable composites by including the influence of manufacturing imperfections, such as resin rich areas and ply-thickness variations. Laminate composition was characterised by optical microscopy and their cured shapes measured using a Peak Motus motion analysis system. The FE model accurately predicts observed differences between laminate curvature in the two stable states. Localised reversal of curvature resulting from through-thickness shear stress is also predicted. Structural response to thermal loading was experimentally characterised showing a temperature dependent deflection rate and a residual curvature caused by non-reversible residual stresses. FE-predictions show good agreement with experiment over the range 20–110 °C. The presented data highlights the importance of manufacturing processes and materials selection in the design of thermally stressed multi-stable composite structures.

© 2009 Elsevier Ltd. All rights reserved.

1. Introduction

Bistable composite laminates have been proposed as a method to generate novel shape changing (or ‘morphing’) structures within a range of engineering sectors such as aerospace and automotive [1,2]. The interest in bistable composites stems from the fact that they are able to sustain significant changes in shape without the need for a continuous power supply [3–7]. Bistable composite laminates are relatively thin unsymmetric laminates, commonly $[0_n/90_n]_T$, which have been cured at elevated temperature [8]. Such composites are multi-stable and exhibit as at least two distinct structurally stable shapes as a result of anisotropic thermal expansions of the composite plies creating a residual stress field during manufacture [8–10]. To induce snap-through from one stable state to another, actuator materials such as shape memory alloys and piezoelectric materials have been employed [4,5,7,11]. Many factors influence the cured shape of bistable laminates including lay-up and material selection [12,13]. In addition these laminates will inevitably contain imperfections from the manufacturing process. Common imperfections from the idealised models used to predict their behaviour include; variations in ply-thickness, compaction, fibre fraction and ply-angle. It has been shown that small variations in ply-angle can alter the behaviour of bistable laminates during

post-cure cooling [14]. However, little is known relating variations in composition and architecture to laminate behaviour.

Regions of locally reversed curvature which are seen near the corners and edges of bistable laminates are not currently predicted by analytical methods [15]. While localised variation in curvature has been predicted using commercial finite element software [16], no comments on the likely physical causes or comparison with experimental measurement of the phenomenon was made.

For the potential application areas, it is likely that multi-stable structures will be exposed to wide ranging thermal conditions, which will affect their performance and stable shapes. For example, during a typical passenger jet flight cycle the temperature may vary in the range –60 °C to 40 °C [17] and to operate reliably it is vital that the response of these laminates is well understood and may be accurately predicted. ‘Active laminates’ have also been proposed with internal heat sources and are formed using materials with different coefficient of thermal expansion (CTE). These have been used to produce a shape change in fibre-metal composites with a layer of low CTE carbon fibre reinforced polymer acting as an electrical resistance heater and to induce bending [18,19]. Recent work has also developed a Controlled Behaviour Composite Material (CBCM), in which the different thermo-mechanical properties of the composite components to induce a change in shape of a structure [20].

The aim of this paper is therefore to characterise the composition and architecture of bistable laminates and their structural response under a range of temperature conditions to aid in the

* Corresponding author. Tel.: +44 1225386524.

E-mail address: p.f.giddings@hotmail.co.uk (P.F. Giddings).

URL: <http://www.bath.ac.uk/mech-eng> (P.F. Giddings).

design of morphing structures which are likely to experience different thermal environments. This paper will use commercial FE software ANSYS V11.0 to develop models of bistable laminates including full three dimensional stress fields in order to accurately predict cured shape and structural response to thermal loading. The proposed model will also include manufacturing imperfections of manufactured composites determined by optical microscopy.

2. Methodology

2.1. Laminate composition and cured shape measurement

$[0/90]_T$ and $[-30/60]_T$ T800/M21 laminates were manufactured using a single-dwell autoclave cure cycle as specified for the M21 resin system. After trimming to remove both resin-poor areas and defects introduced by thermocouple placement the $[0/90]_T$ and $[-30/60]_T$ laminates measured 75 mm \times 75 mm and 150 mm \times 150 mm respectively. Since the laminates were placed on a flat metallic surface within the autoclave, the side in contact with the surface has a smooth finish while the opposite side has a thin layer of resin which bleeds from the top ply and cures on the surface. The influence of this thin resin layer will be included within the model to be discussed in this work. To characterise the resin layer and mean-ply-thickness, optical microscopy specimens of both laminates were prepared from the trimmed material, set in optical microscopy resin and digitally photographed using a Nikon Eclipse Iv150 optical microscope with a Qimaging 3.3RTV digital camera attachment. Mean ply-thickness of each specimen was calculated using image processing software for use in material properties specification for subsequent FE modelling.

Cured shape of the 75 \times 75 mm² $[0/90]_T$ sample at room temperature of 22 °C was assessed via laser profilometry, generating 3D-coordinates defining the laminate surface. A Scantron Proscan 2000 laser profilometer was used to record laminate surface height relative to a datum-plane at nodes on a 300 μ m grid with a resolution of 1 μ m over the measurement range. These raw data were then normalised against the datum-plane to create the surface-coordinates of the deformed laminate in both stable states. The cured shape of the $[-30/60]_T$ laminate at room temperature of 22 °C was measured using a Peak Motus (v. 8.5, Vicon, USA) motion analysis system to provide a non-contact measurement of the spatial-coordinates of reference-points applied to the laminate. Coordinates produced are irregularly spaced across the laminate surface, creating three column-vectors x , y and z . Irregularly spaced spatial-coordinates were imported into MATLAB and the Delaunay triangulation of those data determined to form an irregular surface-mesh. A continuous surface of the form $Z_i = f(X_i, Y_i)$ was fitted to this mesh using spline-based interpolation [21] to generate regularly spaced surface-coordinates. The matrix $[X_i, Y_i, Z_i]$ therefore describes the interpolated surface-approximation to the experimental data.

2.2. Thermal deformation

The experimental analysis of the laminate was performed in order to determine structural response to externally imposed thermal loading. For the thermal experiments a $[0/90]_T$ laminate with a higher aspect ratio (250 mm \times 80 mm) was used to exaggerate the change in curvature with temperature. This was carried out utilising standard motion analysis techniques described in Bowen et al. [7]. The laminate was balanced on a small metal block inside a Gallenkamp vacuum oven so that the front edge of the laminate lay on the xz -plane parallel with the plane of the oven door. A type-K thermocouple was attached to a separate laminate to allow accurate temperature measurement without imposing additional mechanical loading to the test-laminate.

A digital video camera recorder (Sony DCR-TRV 900E, Sony Corporation, Japan) was positioned perpendicular to the xz -plane. The camera was located 2.46 m from the laminate edge at the height of the middle of the oven and operated at 50 fields per second. To allow accurate scaling of images a rectangular calibration object of 303 mm \times 247 mm was located at the back of the oven (130 mm behind the front edge of the laminate). The camera view was restricted just outside the calibration object. The calibration object dimensions were scaled to the front edge of the laminate using trigonometry. Oven temperature was increased from room temperature, with video clips of the laminate taken at 10 °C intervals between 30 °C and 170 °C. Video images were acquired by briefly opening the oven door when the laminate had reached the required temperature. The video clips at each temperature reading were subsequently captured to a computer. The edge of the bent laminate, and the four corners of the calibration object, were manually digitised on Peak Motus[®]; achieved by using a mouse to select 33 points at the edge of the laminate in a random fashion.

Despite careful set up, a slight roll (-0.6°) of the camera was noticed during digitising and this was corrected by rotating the coordinate system accordingly within Peak Motus[®] software. The digitised area consisted of 1440 \times 1152 pixels, resulting in an effective resolution of digitisation of ~ 0.6 mm in both horizontal and vertical directions. After the scaling and reconstruction, the raw coordinates of 33 points were exported to Excel[®] software. A fifth polynomial trend line was applied to the raw coordinates in order to recreate the profile of the laminate in each condition.

2.3. Finite element modelling

Predictions of cured shape and response to thermal loading for the manufactured laminates were made using the FE software ANSYS 11.0. Models were created using the 20-node brick element SOLID186 which allow layers to be defined through the element thickness. SOLID186 elements use quadratic displacement functions to approximate displacement between nodes improving accuracy for highly curved geometries. Material within a layer and the orientation of any anisotropic properties may be varied between layers to accurately model composites without increasing the number of elements used.

The mean-ply-thicknesses determined by optical microscopy were entered as layer thicknesses with corresponding ply-orientations in the SOLID186 element. To fully represent the architecture of the laminates the excess resin layer was included in the element definition. The reduction in mean in-plane stress resultants caused by local edge-effects at boundaries of discontinuities in the resin layer was approximated by reducing the Young's modulus of the layer by 50%.

The materials properties of the cured T800/M21 pre-preg material and resin layer are shown in Table 1 with typical composition for the $[0/90]_T$ laminate shown in Table 2, where subscripts 1 and 2 denote longitudinal and transverse direction in the plane of the fibre and 3 the thickness direction. Subscript r denotes properties of the bulk M21 resin system.

Laminates were modelled and meshed using SOLID186 elements of aspect ratio five for all models. A global change in temperature of (T) was applied to all nodes in the model to simulate a cool down from the 180 °C cure temperature to a temperature matching the relevant experimental conditions. It is important to note that the NLGEOM option of ANSYS static solution was implemented to include geometric non-linearities in the calculation of laminate deformation; NLGEOM specifies the use of rotated element coordinate system in the formulation of the element stiffness matrix.

Two types of FE models were developed (Table 2). Firstly an 'idealised model' which used the laminate composition based on

Table 1
Elastic properties of 268gsm⁻¹ T800/M21 material.

| Property | Value |
|--|--------|
| E_1 (GPa) | 172 |
| E_2, E_3 (GPa) | 8.9 |
| G_{12} and G_{13} (GPa) | 4.2 |
| G_{23}^* (GPa) | 0.0225 |
| V_{12}^-, V_{13} | 0.35 |
| V_{23}^* | 0.01 |
| α_1 (1×10^{-7}) | -0.9 |
| α_2 and α_3 (1×10^{-5}) | 2.65 |
| E_r (GPa) | 1.5 |
| ν_r | 0.4 |
| α_r (1×10^{-5}) | 9 |
| Density (kg m^{-3}) | 1072 |

* Indicates values calculated using stress-strain relations described in [22].

Table 2
Mean and standard deviation (σ) of ply and total laminate thickness for [0/90]_T laminates made from 268gsm M21/T800.

| | Idealised model | Improved model | |
|----------------|-----------------|----------------|----------|
| | Thickness (mm) | Thickness (mm) | σ |
| 0° Ply | 0.25 | 0.255 | 0.013 |
| 90° Ply | 0.25 | 0.233 | 0.018 |
| Resin layer | 0 | 0.017 | 0.021 |
| Total laminate | 0.5 | 0.515 | 0.045 |

the nominal ply-thickness (0.25 mm) used to fabricate the laminates and did not include the resin layer. The idealised model required a temporary mechanical force to be applied during the first 0.1 °C of cooling to allow convergence to the cylindrical states. The 'improved model' used the data from the optical microscopy to capture more precise details and mean-ply-thickness and the presence of the resin rich layer. The 'improved model' enabled convergence to the cylindrical states without externally imposed imperfections or loads, in contrast to work by previous investigators [2,4,23]. No external loads or imperfections were required since the resin layer was a sufficient imperfection to achieve convergence. The stable cylindrical state with the largest value of maximum deflection was designated State A; this coincided with the state where the resin layer lies is on the concave surface. State B is the secondary state, showing reduced maximum deflection and the resin layer lies on the convex surface.

Once the solution converged to an initial first stable state (State A) it was necessary to 'snap' the bistable laminate to the second stable state (State B) to fully determine the shape profile of both states. In order to achieve this within the FE model a displacement constraint was applied to the corner nodes of the laminate. Nodes were displaced to a value equal in magnitude but of opposite sign to their displacement in State A. The constraint was only applied in the z-direction and nodes were free to move in the plane normal to the z-direction. Once the displaced solution converged, the displacement constraint was removed and the model relaxed into stable State B. In each state the calculated through-thickness shear stresses (γ_{xz} and γ_{yz}) in the rotated element coordinate system were read to an output file and plotted against the corresponding nodal z-coordinate. The element coordinate system must be selected to correctly assess the stress acting through the laminate thickness and not those acting in the xz-plane of the global coordinate system.

In order to compare FE-predictions to experimentally measured laminate shapes the deformed nodal coordinates were calculated within ANSYS by summing undeformed nodal coordinates with the respective displacements in the three orthogonal directions. The surface fitting procedure described in Section 2.1 was used

to create a regularly spaced matrix of laminate surface coordinates as the calculated nodal coordinates were not regularly spaced in the xz-plane.

To determine the response of the laminates to thermal load using FE, the cured shape at room temperature (State A) was initially determined, as previously described. Gravity loading was applied with an acceleration of 9.81 m s⁻¹ acting on all nodes within the laminate since the laminate was held horizontally during the thermal experiments. With gravity loading applied, a temperature constraint on all nodes was applied to predict deflection and shape profile at each experimental data point. Nodal coordinates for all nodes at the free-edge of the laminate ($x = 80$ mm) were calculated within ANSYS for comparison with the experimental data. The maximum nodal displacement was plotted against laminate temperature and a linear trend line fitted to the data.

3. Results

3.1. Laminate composition

Fig. 1 shows typical images from optical microscopy of a [0/90]_T laminate. The nominal thickness of the initial composite pre-preg was 0.25 mm, suggesting an idealised laminate thickness of 0.5 mm. The thickness of the total laminate and individual plies differ from idealised values in the range $\pm 6\%$. An uneven layer of resin on the uppermost surface of the laminate is also visible in Fig. 1, the lower face is pressed against the composite tool during curing and therefore has very little surface texture. The observed resin layer varies randomly in thickness between negligible thickness and 0.08 mm over the entire surface of the laminate.

Table 2 shows the mean and standard deviation of ply-thickness and total laminate thickness for the tested laminates. The mean values presented in Table 2 were used to specify layer thickness values within the 'improved model' and SOLID186 element formulation.

The cured shapes of one [0/90]_T laminate measuring 75 mm \times 75 mm and a second [-30/60]_T measuring 150 mm \times 150 mm were predicted using the FE model. Fig. 2 shows cured shape of the [0/90]_T 75 \times 75 mm² laminate in State A (resin layer on the concave lower surface) with maximum deflection (D_{max}) indicated. D_{max} is defined in this paper as the maximum displacement in the z-direction relative to the centroid of the undeformed laminate. Fig. 2 has the experimental shape profile along with the overlaid FE-predicted profile, indicating good agreement. Table 3 summarises all the experimental and modelling data and compares the measured maximum deflections of the [0/90]_T and [-30/60]_T laminates with those predicted by the 'idealised' and 'improved' FE models.

3.2. Cured shape and finite element prediction

Experimentally measured maximum deflection (D_{max}) in States A and B were not of equal magnitude in all laminates. States A and B should theoretically be of equal magnitude if the individual ply-thicknesses were exactly 0.25 mm. In both cases the D_{max} was the greatest in State A, in which the thermal contraction of the excess resin layer acts to increase D_{max} by increasing curvature. It was observed during manufacture that all laminates cooled into State A immediately after curing. For the 'idealised model', in which the plies are of equal thickness and do not contain a resin layer, the magnitude of D_{max} is equal in States A and B (Table 3) and agreement with experimentally measured values is relatively poor. The 'improved model' showed excellent qualitative agreement with experiment and both states were accurately modelled. The largest error between FE-predictions of the 'improved model' and experiment was observed for D_{max} on the surface of the [-30/60]_T

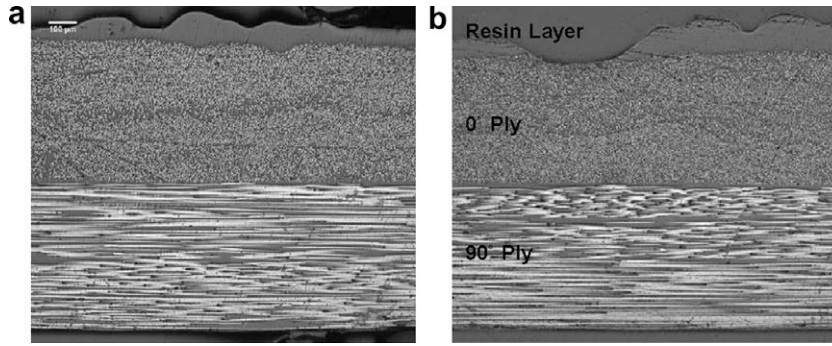


Fig. 1. Two sample images showing composition for T800/M21 [0/90]_T laminate. White scale bar in (a) is 100 μm and both images are at same magnification.

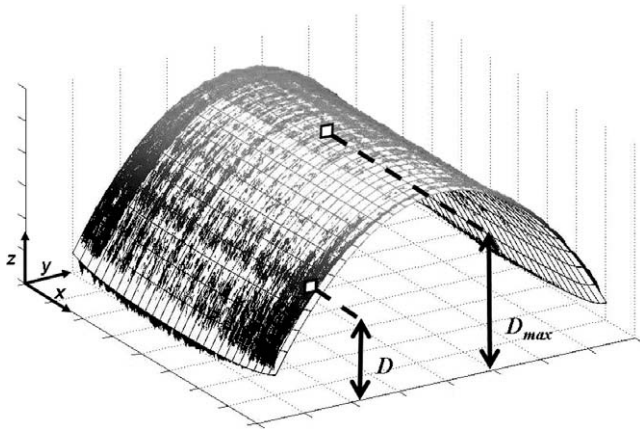


Fig. 2. State A cured shape for 75 × 75 mm [0/90]_T laminate, experimental surface with overlaid FE-predicted mesh.

laminate with FE underestimating D_{max} by 6.8%. By comparison, in this extreme case, the ‘idealised FE’ solution underestimated D_{max} by 73.5% with the predicted laminate adopting a saddle shape and not the experimentally observed cylindrical curvature. As seen in Fig. 2 the [0/90]_T laminate shape profile was very well predicted by the improved model, with a peak error of 3.3% and an accurate reproduction of the local reversal of curvature near the edges and corners of the laminate. It should also be remembered that the ‘improved model’ converged to State A without the use of temporary forces in the solution process, thus reducing user intervention in the FE-solution process.

Fig. 3 shows measured and FE-predicted (‘improved model’) values for D along the $x = 150$ mm edge of the [−30/60]_T laminate, and the inset shows an expanded view of this data for the corner region near $y = 150$ mm. D is height of the laminate as a function of distance in the y -axis, as defined in Fig. 2. The observed corner effect, seen as a reversal of local curvature near $y = 0$ and $y = 150$ mm is predicted by the FE model. Through-thickness shear stress γ_{xz} (expressed in the deformed element’s coordinate system) is also plotted in Fig. 3 and the inset. This shows that the regions of reverse curvature also experience an increased through-thickness

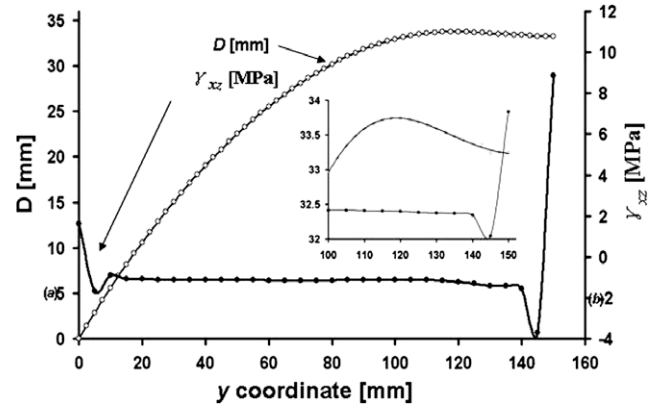


Fig. 3. xz -shear stress (γ_{xz}) and deflection (D) at the $x = 150$ mm of [−30/60]_T laminate free-edge as a function of z -coordinate, expanded view of the corner region (inset).

shear stress in order to maintain equilibrium under the imposed boundary conditions at a free-edge. Although not shown in this paper, it was observed that localised peaks in the other through-thickness shear stress γ_{yz} exhibited a similar variation in the corner regions to those seen for γ_{xz} .

The improved FE model captured the edge and corner effects of both the [−30/60]_T and [0/90]_T laminates. Good agreement was observed between model predictions and measured values (Table 3), including the reversal of curvature, with the error between FE and experiment remaining constant in the corner regions. For example, Fig. 4a shows the measured surface profile (dots) of the [−30/60]_T laminate in State B, with the FE prediction (mesh) superimposed for comparison; both surfaces reverse curvature with the FE-surface following the experimental data well. Fig. 4b shows the same region of the FE-predicted surface and shaded to illustrate the magnitude of the in-plane shear stress (γ_{xy}). The region of maximum γ_{xy} corresponds to the maximum reversed curvature in the y -direction and large variations of both γ_{xz} and γ_{yz} (see Fig. 3 and inset). In contrast to FE models, this three dimensional stress state is not considered in the current analytical techniques and therefore edge-effects are not predicted.

Table 3
Maximum deflection (D_{max}) for States A and B of 75 × 75 mm² [0/90]_T and 150 × 150 mm² [−30/60]_T laminates.

| Bistable laminate | Experimental data (mm) | | Idealised model (mm) | | Improved model (mm) | |
|-----------------------|------------------------|---------|----------------------|---------|---------------------|---------|
| | State A | State B | State A | State B | State A | State B |
| [090] _T | 5.12 | 3.55 | 3.76 | 3.76 | 4.98 | 3.53 |
| [−30/60] _T | 45.11 | 38.22 | 11.95 | 11.95 | 42.04 | 33.49 |

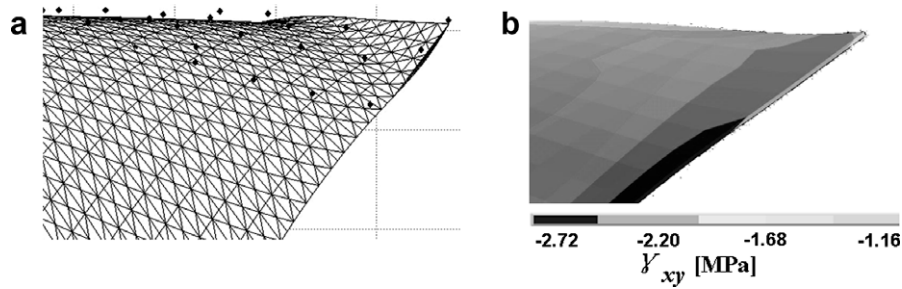


Fig. 4. Close-up view of corner region: FE-predicted mesh with superimposed experimental data points (a) and surface plot of γ_{xy} -shear stress (γ_{xy}) (b) for $[-30/60]_T$ laminate in State B.

3.3. Response to thermal load

Fig. 5 shows laminate profile under imposed thermal load; as laminate temperature increases D_{max} decreases as the laminate flattens. At low temperature, the laminate has a positive curvature in the x -direction, however, as the temperature increases regions of negative curvature develop at the edges of the laminate as indicated at point (a) in Fig. 5.

Fig. 6 shows the measured maximum deflection of the laminate (D_{max}) for each sample temperature along with the corresponding FE-predictions ('improved model'); a fifth order polynomial was fitted to the experimental data ($R^2 = 0.99$) while a linear trend line was adequate ($R^2 = 0.99$) to fit to the FE data. The relationship between laminate temperature and D_{max} for the experimental data is more complex than predicted by the FE model. During heating, D_{max} initially increases at similar rates in both experimental and FE data, however at approximately 50 °C the rate of change of D_{max} with respect to temperature reduces significantly. As the laminate temperature increases beyond 120 °C the rate of change of D_{max} with temperature increases once more; this change in behaviour corresponds with the observed negative curvature at the edge of the laminate, point (a) in Fig. 5.

Epoxy resins are known to soften (reduced coefficient of thermal expansion (CTE), elastic and shear moduli) in the range of 50–120 °C [24]. At approximately 120 °C the CTE increases once more although the elastic and shear moduli continue to decrease. Though no specific information relating to the M21 system used here has been published, data reported in [24] relate to a structural epoxy used in composite construction thought to be similar to M21.

Gravity loading in conjunction with the softened matrix cause the ends of the laminate to reverse curvature or "sag" toward the $z = 0$ plane. Despite the observed non-linearities in the laminate's response to thermal loading the FE-predictions remain within 10% of experimental values in the range 22–109 °C. Thereafter percentage errors rise as laminate deformation approaches zero, how-

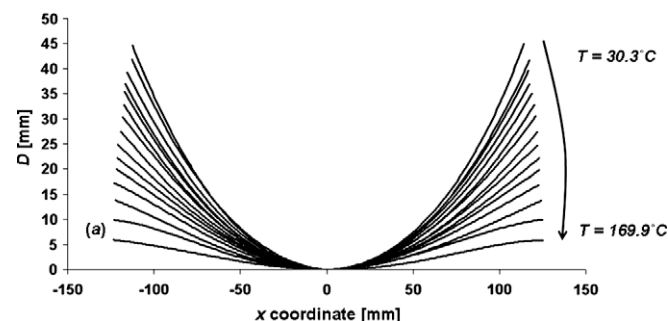


Fig. 5. Variation in laminate profile between 30.3 and 169.9 °C.

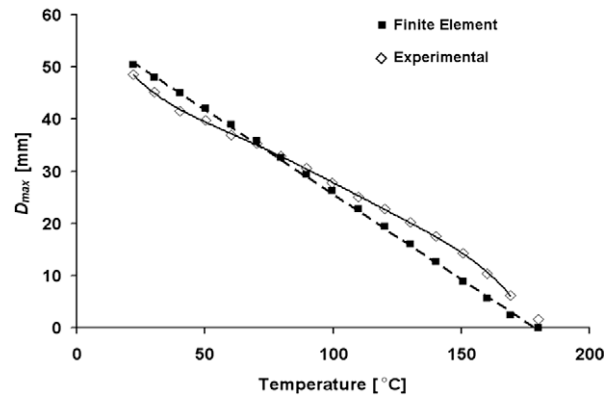


Fig. 6. Measured and FE-predicted values for D_{max} as a function of laminate temperature for $250 \times 80 \text{ mm}^2$ $[0/90]_T$ T800/M21 laminate.

ever absolute error remains less than ± 5 mm over the entire temperature range.

It was noted that although the laminate approached the cure temperature of 180 °C, the laminate curvature did not reduce to zero as expected. The gradient of the D_{max} versus temperature line was calculated for the experimental data by the finite difference method [25] between 150.7 and 169.9 °C and the value of D_{max} at a laminate temperature of 180 °C was approximated using linear extrapolation. A predicted D_{max} value of 1.57 mm at 180 °C shows that a significant residual stress field remains within the laminate. The authors suggest that this residual curvature (once gravity loading has been corrected for) could serve as a convenient measure of the non-reversible residual stresses present within thin asymmetric composites. It is likely that the residual stress field is comprised of superposed stresses resulting from chemical shrinkage, tool interaction [10,26] and differential curing through the thickness of the laminate.

4. Conclusion

This paper has characterised the composition and architecture of bistable laminates and their structural response under a range of temperature conditions to aid in the design of morphing structures. To capture manufacturing imperfections the thin cross-ply composite laminates were characterised using optical microscopy in conjunction with digital image processing. The presence of an excess resin layer was identified and ply-thicknesses within two-ply cross-ply laminates measured and compared to idealised laminate models. Both individual ply and total laminate thickness were seen to deviate by up to 6% from idealised values.

Cured shapes for a $75 \times 75 \text{ mm}$ $[0/90]_T$ were measured using laser profilometry and those a $150 \times 150 \text{ mm}$ $[-30/60]_T$ laminate were determined via Peak Motus. Peak deflection (D_{max}) was not

equal in both stable states, rather a dominant state was observed in which D_{max} was greater; this state corresponded with the excess resin layer being at the uppermost surface when the laminate curvature was concave. Localised reversal of curvature near the edges and corners of the laminates was observed with both effects strongest with the laminate in State B.

A finite element (FE) model including the observed laminate composition was described and implemented within commercial FE software ANSYS V11.0 to predict the cured shapes of the test-laminates. This improved FE model captured the inequality in States A and B deflection to within 3–7% as compared with errors ranging between 7% and 73% for FE models using idealised laminate composition. The improved model converged to the stable state of greatest curvature without need of imposed imperfections to aid convergence. The 'improved model' enabled convergence to the cylindrical states without externally imposed imperfections or loads, in contrast to work by other investigators.

The FE model was also able to predict edge and corner effects which were shown to be related to localised increases in the through-thickness components of shear stress γ_{xz} and γ_{yz} . These effects are not possible to predict using the plate theory prevalent in the analysis of bistable laminates [13,27,28]. Promising work continues to be presented in the field of shell theories to predict bistable behaviour [29], however, these techniques are not yet established in this field.

The response of a 250×80 mm $[0/90]_T$ laminate to an imposed thermal load was investigated by measuring laminate deflection during heating using motion capture techniques. The rate at which deflection increased in response to a temperature change was not linear as expected, but rather influenced by temperature dependent mechanical properties of the resin system and the resulting deflection under gravitational load. The deflection at cure temperature was extrapolated from the experimental data and a residual deflection of 1.57 mm predicted. This deflection at cure temperature indicates the presence of a residual stress which is not fully relaxed by reheating, resulting from a superposition of stress fields created by chemical, mechanical and thermal effects during the cure cycle. The improved FE model was able to predict the deflection of the laminates during the heating cycle to within 10% over the range 20–110 °C and demonstrates the importance of developing models that capture manufacturing imperfections such as changes in ply-thickness and resin rich areas. The ANSYS FE model described in this work is of interest as a design and scoping tool for multi-stable structures operating within the range 20–110 °C, however further investigation into the effects of the temperature dependent behaviour of the polymer matrix is necessary to extend their operating envelope.

References

- [1] Schultz MR. A concept for airfoil-like active bistable twisting structures. *J Intell Mater Syst Struct* 2008;19(2):157–69.
- [2] Mattioni F, Weaver PM, Potter KD, Friswell MI. Analysis of thermally induced multistable composites. *Int J Solids Struct* 2008;45(2):657–75.
- [3] Schultz MR, Hyer MW. Snap-through of unsymmetric cross-ply laminates using piezoceramic actuators. *J Intell Mater Syst Struct* 2003;14(12):795–814.
- [4] Schultz MR, Hyer MW, Williams RB, Wilkie WK, Inman DJ. Snap-through of unsymmetric laminates using piezocomposite actuators. *Compos Sci Technol* 2006;66(14):2442–8.
- [5] Gude M, Hufenbach W. Design of novel morphing structures based on bistable composites with piezoceramic actuators. *Mech Compos Mater* 2006;42(4):339–46.
- [6] Giddings P, Bowen CR, Butler R, Kim HA. Characterisation of actuation properties of piezoelectric bi-stable carbon-fibre laminates. *Compos Part A – Appl Sci Manuf* 2008;39(4):697–703.
- [7] Bowen CR, Butler R, Jervis R, Kim HA, Salo AIT. Morphing and shape control using unsymmetrical composites. *J Intell Mater Syst Struct* 2007;18(1):89–98.
- [8] Hyer MW. Some observations on the cured shape of thin unsymmetric laminates. *J Compos Mater* 1981;15(MAR):175–94.
- [9] Kim KS, Hahn HT. Residual-stress development during processing of graphite epoxy composites. *Compos Sci Technol* 1989;36(2):121–32.
- [10] White SR, Hahn HT. Process modeling of composite-materials – residual-stress development during cure. 1. Model formulation. *J Compos Mater* 1992;26(16):2402–22.
- [11] Dano ML, Hyer MW. SMA-induced snap-through of unsymmetric fiber-reinforced composite laminates. *Int J Solids Struct* 2003;40(22):5949–72.
- [12] Dano ML, Hyer MW. The response of general unsymmetric laminates to simple applied forces. In: *Proceedings of the eighth Japan-US conference on composite materials*; 1999. p. 179–88.
- [13] Jun WJ, Hong CS. Cured shape of unsymmetric laminates with arbitrary lay-up angles. *J Reinf Plast Compos* 1992;11(12):1352–66.
- [14] Hamamoto A, Hyer MW. Nonlinear temperature–curvature relationships for unsymmetric graphite–epoxy laminates. *Int J Solids Struct* 1987;23(7):919–35.
- [15] Schlecht M, Schulte K, Hyer MW. A comparative study for the calculation of the temperature dependent shapes of unsymmetric laminates based on finite element analysis and extended classical lamination theory. *Mech Compos Mater* 1995;31(3):247–54.
- [16] Dano ML, Hyer MW. Thermally-induced deformation behaviour of unsymmetric laminates. *Int J Solids Struct* 1998;35(17):2101–20.
- [17] Diaconu CG, Weaver PM, Mattioni F. Concepts for morphing airfoil sections using bi-stable laminated composite structures. *Thin-Walled Struct* 2008;46(6):689–701.
- [18] Asanuma H, Haga O, Imori M. Development of high performance CFRP/metal active laminates. *JSME Int J Ser A – Solid Mech Mater Eng* 2006;49(1):32–7.
- [19] Asanuma H, Haga O, Ohira J, Takemoto K, Imori M. Fabrication of CFRP/Al active laminates. *JSME Int J Ser A – Solid Mech Mater Eng* 2003;46(3):478–83.
- [20] Drobez H, L'Hostis G, Gautier KB, Laurent F, Durand B. A new active composite. *Smart Mater Struct* 2009;18(2):1–7.
- [21] Sandwell DT. Biharmonic spline interpolation of geos-3 and seasat altimeter data. *Geophys Res Lett* 1987;14(2):139–42.
- [22] Hyer MW. *Stress analysis of fibre reinforced composite materials*. Boston, Mass: WCB/McGraw-Hill; 1998.
- [23] Hufenbach W, Gude M, Kroll L. Design of multistable composites for application in adaptive structures. *Compos Sci Technol* 2002;62(16):2201–7.
- [24] Schlecht M, Schulte K, Hyer MW. Advanced calculation of the room-temperature shapes of thin unsymmetric composite laminates. *Compos Struct* 1995;32(1–4):627–33.
- [25] Stroud K. *An engineering mathematics*. London, UK: MacMillan Education Ltd.; 1987.
- [26] White SR, Hahn HT. Process modeling of composite-materials – residual-stress development during cure. 2. Experimental validation. *J Compos Mater* 1992;26(16):2423–53.
- [27] Hyer MW. Calculations of the room-temperature shapes of unsymmetric laminates. *J Compos Mater* 1981;15(JUL):296–310.
- [28] Ren LB, Parvizi-Majidi A. Cured shape of cross-ply composite thin shells. *J Compos Mater* 2003;37(20):1801–20.
- [29] Pirrera A, Weaver PM. Geometrically nonlinear first-order shear deformation theory for general anisotropic shells. *AIAA J* 2009;47(3):767–82.